Oliver S. Gibson
Department of Mechanical Engineering and Materials Science,
Duke University,
Durham, NC 27708
e-mail: oliver.gibson@duke.edu

Chris Knotek
Department of Mechanical Engineering and Materials Science,
Duke University,
Durham, NC 27708
e-mail: christopher.knotek@duke.edu

Lawrence Virgin
Professor
Department of Mechanical Engineering and Materials Science,
Duke University,
Durham, NC 27708
e-mail: l.virgin@duke.edu

Earl Dowell[1]
Professor
Department of Mechanical Engineering and Materials Science,
Duke University,
Durham, NC 27708
e-mail: earl.dowell@duke.edu

Buckling of a Vertically Mounted Cantilevered Plate Under Static Torsional Corner Loads—Experiment and Theory

The results of an experimental study on the buckling of a vertically cantilevered plate under corner twisting forces are reported. In this configuration, an interesting and somewhat counter-intuitive behavior is observed in which a laterally loaded slender panel exhibits a subtle instability characterized by nonlinear out-of-plane corner deflections. This is one of the few studies in the literature that investigates the buckling of cantilevered plates and appears to be the only experimental study of buckling under twisting loads, i.e., loading the plate with point loads at the free corners and in opposite directions. This paper discusses the practical aspects of experimental verification and methodology and evaluates the effect of the plate aspect ratio (AR) on the nondimensional buckling load in this configuration. In addition, experimental results are compared to finite element analysis (FEA) simulations performed on accessible software. There is generally good agreement between the experiment and the finite element simulation for the change of buckling load with plate aspect ratio. The nondimensional buckling load appears to decrease asymptotically with increasing aspect ratio, though the correlation between experiment and computation is less consistent as aspect ratio increases due to experimental and computational limitations.
[DOI: 10.1115/1.4056859]

Keywords: buckling, computational mechanics, elasticity, experimental mechanics, structures

1 Introduction

Buckling is one of the most important physical phenomena in structural engineering, often providing limiting design constraints, especially in aerospace applications. Much of the early literature is well described in the classic text by Timoshenko and Gere [1]. Publications continue to appear with particular emphasis on buckling due to thermal stresses for structures operating at high temperatures and on buckling for devices built at the nanoscale. See, for example, the paper by Lachut and Sader [2] and the literature cited therein. Note also that the paper by Lachut and Sader is one of the few that treats a cantilevered plate for the case of in-plane loads. Even at the nanoscale, continuum theories are often used and provide physically meaningful results. There is also literature where buckling is used to provide new and desirable shapes and beneficial exploitation [3,4], although much of the conventional literature on buckling is devoted to understanding how buckling may be prevented.

The present paper investigates a theoretical finding of Pai et al. [5] and presents a finite element computation comparable to that done by Pai for correlation with the experimental data. The structural configuration is a cantilevered plate with corner twisting loads. The correlation between experiment and theory is generally good, especially given the physical complexity of the buckling phenomenon. In many classical studies of buckling, e.g., a straight Euler beam or the generalization to a plate under in-plane compressive loads, the critical load can be found from a linear eigenvalue analysis, since there is no out-of-plane deformation until buckling occurs. It has been well established that imperfections due to deviations from a straight beam or perfectly flat plate may lead to further complications and must be treated by a nonlinear theory [6].

In the present case, even small lateral loads lead to nonlinear out-of-plate deflections and buckling can occur when the deformations are well into the nonlinear range. Because the physical phenomenon is inherently nonlinear, the approach to buckling, the onset of buckling, and the deformation after (post) buckling are considered here in both the experiment and the computations. The application of the loads in opposite directions (causing a twisting effect) leads to the appearance of in-plane stresses, and these are the underlying cause of buckling. Finally, it is noted that substantial literature also exists on snap buckling or dynamic buckling [6–8], but this aspect of buckling is not pursued in the present study.

The current paper provides both experimental and computational evidence that a cantilevered plate can buckle under a twisting load. The previous computations of Pai et al. [5] now well establish this surprising result by the present experimental and computational work. The various sections of the paper are Introduction (Sec. 1) including the Problem Statement (Sec. 1.1) and Motivation (Sec. 1.2); Experimental Methods (Sec. 2) including Experimental Setup (Sec. 2.1), Experimental Procedure (Sec. 2.2), and Uncertainty and Limitations (Sec. 2.3); Computer Simulation Methods (Sec. 3) including Simulation Motivation (Sec. 3.1), Simulation Setup and Method (Sec. 3.2), and Uncertainty and Limitations (Sec. 3.3); Results (Sec. 4) including Dimensional Load Versus Displacement (Sec. 4.1) and Nondimensional Load Versus Aspect Ratio (AR) (Sec. 4.2), and finally Conclusions and Possible Future Work (Sec. 5).

1.1 Problem Statement.

A vertically cantilevered rectangular plate is clamped at one end and subject to normal, opposing point loads at its two free corners. The corners deflect out-of-plane with progressive nonlinearity, and upon reaching a critical load, the plate buckles. There are three distinct equilibrium configurations:

[1]Corresponding author.

Contributed by the Applied Mechanics Division of ASME for publication in the Journal of Applied Mechanics. Manuscript received November 7, 2022; final manuscript received February 3, 2023; published online February 22, 2023. Assoc. Editor: Pedro Reis.

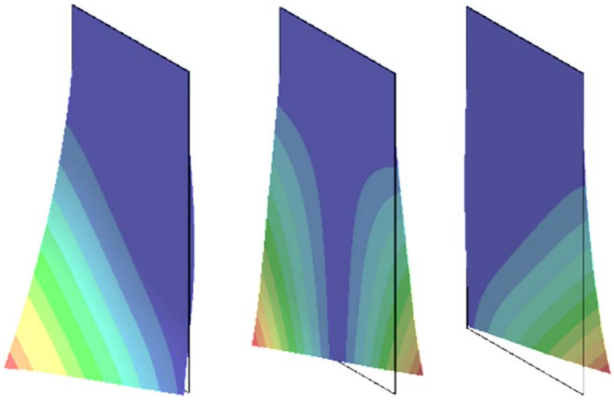

Fig. 1 Typical deflected shapes of the panel: plate buckled forward (left), plate unbuckled (center), and plate buckled backward (right)

one pre-buckling where the corners deflect equally in magnitude but opposite in direction, one where the plate is buckled forward, and one where the plate is buckled backward. In the ideal case of a perfect plate subject to identical opposing corner loads and in-plane gravitational forces, the forward and backward buckling modes would be expected to have anti-symmetric displacements. Initially, the plate twists with a small deflection, but then becomes concave and buckles in one direction upon reaching the critical load. Buckling direction depends on plate imperfections and the loading sequence near the buckling point. See Fig. 1 for computer-simulated states of the plate.

1.2 Motivation. The buckling phenomenon of a cantilevered plate in this loading case was predicted by Pai et al. with the finite element analysis (FEA) software ABAQUS [5]. Their formulation was based on a geometrically exact formulation. The present paper investigates this theoretical finding from an experimental perspective and characterizes the force-deflection relations, especially the nondimensional relationship between buckling load and AR. Additionally, experimental data will be compared to ANSYS FEA simulations conducted by the present authors. Predicting the buckling load and deflection of cantilevered plates directly applies to modeling cantilevered elastic structures, such as aircraft wings. Data were also obtained for a horizontally cantilevered plate, where gravity introduces a non-trivial asymmetry to the deflection and alters the buckling behavior of the plate. The horizontal case has symmetry-breaking gravitational forces and will be reported separately.

2 Experimental Methods

2.1 Experimental Setup. Data were collected from three different rectangular 6061 aluminum alloy plates of varying widths and aspect ratios, where the aspect ratio is equal to plate length (a) divided by plate width (b). The nominal plate widths are 2, 5, and 10 in. Note that the actual plate widths are not exactly equal to the nominal widths. See Table 1 for the exact dimensions of the three different plates used in this study.

The thickness of each plate was 1/32 in. (0.794 mm), based on standard stock. Small holes were drilled near the free corners of each plate with a 1.5 mm drill bit. Lines were then drawn on each plate with a marker to indicate the lengths corresponding to different aspect ratios. The terms "front" and "back" regarding the plate and testing rig orientations are arbitrary, but it is helpful to make permanent front and back designations when determining whether the plates and testing rig have an orientation bias in measuring deflection. A perfectly flat plate is expected to deflect anti-symmetrically when the direction of the corner loads is reversed. The maximum aspect ratio of the plates was limited by either the plate length or the available length inside the testing rig. See Fig. 2 for a diagram of the test setup.

Table 1 Experimental plate dimensions

Plate width, b (mm)	Plate width, b (in.)	Maximum AR, a/b
50.01	1.96875	10
126.21	4.96875	4
254.79	10.03125	2

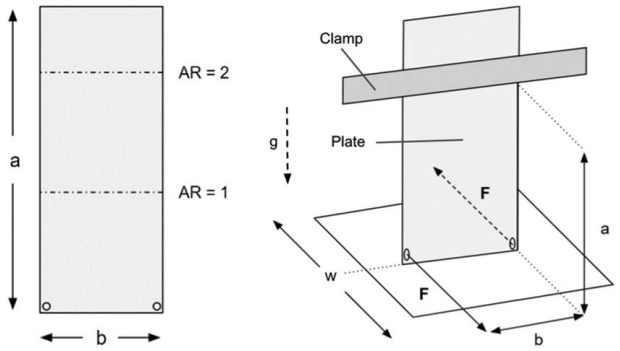

Fig. 2 Schematic diagram of sample test plate (left); diagram of ideal test setup with plate, clamp, point forces *F*, dimensions *a* and *b*, displacement *w*, and gravity *g* (right)

The test rig was constructed of 1-in. thick (25.4 mm) 80/20 aluminum t-slot extrusions. The members were joined with a combination of 3D-printed polylactic acid plastic (PLA) and standard metal t-slot brackets to form a prismatic rig to which a clamp, a ruler, and two low-friction acetal plastic pulleys were fixed. A test plate can then be inserted into the clamp, which consists of two 2.5 in. (63.5 mm) wide 6061 aluminum bars bolted together on either side of the plate. A C-clamp is additionally placed in the middle of the bars to apply pressure more evenly to the plate through the bar clamp. Both the bar clamp and pulleys are adjustable on two axes and are repositioned before each test to ensure the levelness of the setup and perpendicularity of the corner loads to the plate. The maximum plate length inside the extended rig is 35 in. (889 mm), which sets an upper limit on the testable aspect ratios unless plates narrower than 2.5 in. (63.5 mm) are used, which is not recommended due to the disproportionate effect of plate imperfections on nonlinear deflections in small plates. Although the test setup was not bolted to the tabletop, it is believed to be sufficiently rigid and does not appear to move during testing. Several iterations of the testing rig can be seen in Fig. 3.

2.2 Experimental Procedure. A plate is first inserted into the clamp at the selected length. After checking the perpendicularity of the plate to the bar clamp with a square tool, the bolts are tightened, and the C-clamp is added. The bar clamp is then leveled on either

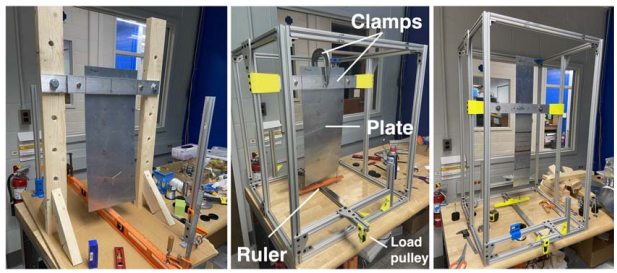

Fig. 3 Wooden rig (left), T-slot structure (middle), and extended T-slot structure (right)

side to ensure that the plate hangs as vertically as possible. Fishing line is looped through the corner holes of the plate and placed over the pulleys, which are finely adjusted so that the string is normal to the plane of the plate. The pulley, axle, and fishing line are then sprayed with WD-40 to reduce friction. The initial no-load position of each plate corner is measured by aligning a 3D-printed plastic slider on the ruler with each corner and reading off the corresponding measurement. This sets the datum point for each corner from which displacements are measured. Mass hangers are then tied to the fishing line.

The manner and order in which mass is added or removed affect the displacement of the plate. Mass should be added slowly to simulate a quasi-static load increase to not perturb the system dynamically. The direction of buckling can be controlled by adding mass preferentially to that side. Masses are always added first and removed last from the side intended to buckle. As the system has some pulley friction, there is a small range of possible equilibrium displacements for each corner. A dynamic disturbance may cause the plate corner to come to rest at any one of the positions in this range, which may vary on the order of a centimeter in the present configuration. For consistency, the outlined measurement technique intends to capture the maximum displacement possible on the buckled side. Preferentially adding load to one side will initially move the buckled corner beyond its equilibrium displacement point. When the load is slowly equalized with the addition of mass on the other side, the buckled corner will return to its maximum equilibrium displacement. Adding mass suddenly can result in dynamic transients that could settle onto any available equilibrium configuration, rather than follow the immediate path.

Two testing procedures were used to obtain plate displacement data (see Fig. 4). The "single loop" method captures only one set of data for each position but is faster and can be done without prior knowledge of the buckling point. The "double loop" method collects data for each position twice but requires approximate prior knowledge of the buckling point before testing and is more time-consuming. These methods are not exhaustive. In the single loop method, mass is added with loading priority to the front of the plate up to the maximum load. Then, the plate is intentionally buckled into the second buckling mode by pulling gently on the masses on the back side of the plate and finding the extreme displacement position for the anti-symmetric mode. Then, the masses are gradually unloaded with buckling priority to the back, meaning that the masses on the front side are always removed first. In the double loop method, masses are loaded with priority to the front side up to the maximum load. Then, masses are removed with priority to the front until a point below the believed buckling load is reached. Masses are then added with priority to the back of the plate up to the maximum load, and the plate should buckle into its second configuration. Finally, all masses are removed with priority to the back. These two loading approaches help identify equilibrium paths and co-existing responses.

2.3 Uncertainty and Limitations. The friction in the pulleys, the variation in the angle of the fishing line relative to the plate, and the variation in the masses contribute to deflection and applied load uncertainties. In a simple system where fishing string attaches two masses over a load pulley from the test rig, it was found that the masses did not accelerate unless the difference in mass between them exceeded 10 g. This friction in the pulleys results in a mild spread in the collected displacement data. When the plate is loaded in the rig and one of the masses is raised and lowered slightly up or down, the corner displacement will change, but the corner may not return to its original position (the greater the friction in the pulley, the greater the range of possible corner displacements for a given loading configuration). Therefore, a careful method of slowly adding and removing masses is recommended to capture only the most extreme corner position within the range of possible values. Pulley friction can be roughly accounted for by absorbing the holding force of the pulleys into the corner loads by adding or subtracting on the order of 10 g to the values of the corner masses.

Ideally, the fishing line is perpendicular to the plane of the plate such that the force from the hanging mass acts in the normal direction. However, the angle of the string may be misaligned, and the range of possible string locations is estimated to be bounded by a 5 deg cone from the normal axis of the plate based on test rig measurements. The actual force perpendicular to the plate is then proportionally reduced by the trigonometric normal component of the plate.

$$F_{\perp} = F_{\text{applied}} * \cos(5\ \text{deg}) = 0.996 * F_{\text{applied}}$$

This results in an estimated maximum 0.4% reduction in the normal force on the plate from the nominal mass over the pulley and indicates that a small, in-plane external force on the plate is present. The mass hangers and mass disks themselves also have variations in their masses. The two 100 g hangers have masses 101.38 g and 100.72 g, which is sufficiently close to 100 g in the scope of the applied loads (often in the hundreds of grams) to be considered negligible. The 100 g mass disks weigh an average of 99.77 g with a standard deviation of 0.52 g. A stack of ten disks has a standard deviation of 1.6 g in a combined distribution, which is also orders of magnitude less than the applied corner forces and is also ignored. A 3D-printed plastic slider helps align the corner of the plate with the correct mark on the ruler, although

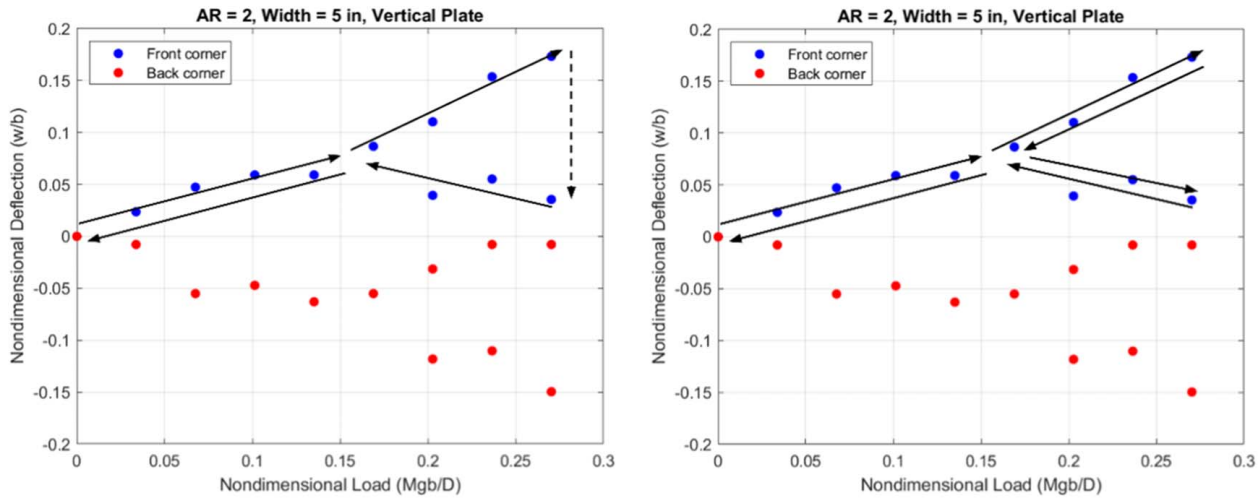

Fig. 4 Single loop method (left) and double loop method (right). Arrows indicate the loading direction and dots show representative experimental data.

the guide itself can twist and wobble, adding a measured ±3 mm of displacement uncertainty.

The greatest source of uncertainty in the experimental system comes from the inherent nature of the buckling behavior. Directly after the buckling point (typically within a mass range of 50 g for the tested plates), the two buckling modes may appear indistinguishable. Lower aspect ratio plates tend to deflect less than higher aspect ratio plates for the same applied load, making buckling difficult to observe without high precision measuring tools. In high aspect ratio plates, there is more uncertainty after the buckling point as the plate deflection is extremely sensitive to increases in load and it is difficult to accurately determine the maximum displacement. The buckling mass of each aspect ratio has an uncertainty of approximately ±50 g determined by the increments of the available masses.

The experimental buckling load is identified as the applied load at which the difference in displacement measurements for the same corner first exceeds 6 mm, at which the measurements given the ±3 mm displacement uncertainty are believed to be distinguishable. This can be found by plotting the range of displacement data against the applied load and identifying the interpolated load where the measured displacement crosses 6 mm.

3 Computer Simulation Methods

3.1 Simulation Motivation. While the experimental method provided measured data on the buckling phenomenon, it is also clear that the limitations of the setup and the non-perfect nature of the tested plates impact the ability to generalize the data. For this reason, it was considered useful to compare experimental results with a commercially available finite element solver code. ANSYS WORKBENCH 2021 was selected for these simulations due to its user interface and licensing accessibility. The goal of these simulations is to compute both plate displacement data and buckling points for any given plate dimension or aspect ratio. Note that simulations were limited only to the nominally 5 in. wide plate (126.21 mm). This plate generally had the clearest experimental data over a range of aspect ratios, up to aspect ratio 4. The nominally 2 in. wide plate deflected too little at low aspect ratios to have easily distinguishable displacement with the present experimental setup, and the simulation software had difficulties handling the excessively large displacements characteristic of the higher aspect ratios. Experimental data from the nominally 10 in. plate were taken at only a few different aspect ratios due to limitations in test rig size.

3.2 Simulation Setup and Method. ANSYS WORKBENCH 2021 features both static "structural" and "eigenvalue" buckling capabilities which can simulate both linear and nonlinear displacements. One documented method of predicting the critical buckling load involves feeding the results of a static structural simulation for a plate subject to a pre-buckling load into an eigenvalue buckling simulation, which will calculate a λ factor that is a load multiplier for a statically applied force. The predicted buckling load is then the multiplier times that load. It is convenient in this case to use an applied load of unity such that the buckling load is simply equal to λ in the corresponding units. To view the displacement of the plate post-buckling, the results of the eigenvalue buckling study are then fed into a second static structural simulation, where the first mode shape calculated in the eigenvalue buckling study is multiplied by a scale factor to form an initial, perturbed, and asymmetric plate geometry. It is unclear how to pick this scale factor, however a value of 0.0001 was used in a different study [9]. This simulation method did not produce buckling load results like the experimental data. Note that the eigenvalue buckling study is only intended to provide results for a geometrically symmetric plate.

Another method was attempted using only a static structural study. One limitation of the static structural study is the inability to calculate post-buckling displacements for a symmetric setup. Thus, adding a small perturbation force was necessary to introduce an asymmetry into the model. The chosen method for doing so was by adding a 0.0098 Newton force (corresponding to 0.001 kg-force or 1 g-force) normal to the plane of the plate exactly at the bottom edge, effectively pre-bending the plate slightly in the forward direction. This allowed the static structural simulation to effectively calculate nonlinear post-buckling displacements. The addition of this perturbation determines the buckling direction of the plate in the simulation. A perturbation force will result in buckling in the same direction as the applied pre-loading force.

Table 2 Summary of experimental and simulation material properties

Property	6061 aluminum alloy (experiment) [10]	ANSYS aluminum alloy (simulation) [11]
Density	2700 kg/m^3	2770 kg/m^3
Young's modulus	68.9 GPa	71 GPa
Poisson's ratio	0.33	0.33
Shear modulus	26 GPa	26.692 GPa

The material for the simulation was selected as an aluminum alloy with software-loaded properties that differed slightly from the 6061 aluminum alloy used in the experiment, although custom properties can be defined by the user. The difference of the physical parameters for the experiment and those used in the finite element computation are small and less than the uncertainty in determining the buckling loads from the experimental data. The relevant properties of the experimental and simulated materials are summarized in Table 2. In future simulations, a custom material could be created that matches the exact properties of the tested 6061 aluminum alloy. See Refs. [10,11].

The model geometry was imported as a .sldprt file from SOLIDWORKS and the plate was modeled with the nominal width of 5 in. (127 mm), not the measured width of 126.21 mm, while the thickness of the plate was modeled as exactly 1/32 in. (0.79375 mm). An additional 2 in. (50.8 mm) was added to the length of the plate model to provide the clamping surface. A mesh with an element size of 5.0 mm was used for all simulations, with all other mesh settings left at their default values. The mesh for each plate appeared nearly square and uniform, with no apparently skewed elements. Each simulation was run for one step with either 250 or 500 sub-steps, depending on the convergence of the solution. The large deflection setting was also enabled, and all other analysis settings were left at default. The number of mesh elements and sub-steps for each simulation are summarized in Table 3.

Each side of the 2 in. (50.8 mm) clamp surface was given a fixed boundary condition to model the boundary conditions imposed by the aluminum clamp in the experimental setup. The effect of gravity was ignored in the simulation as the corner displacements are only a few centimeters from the vertical plane, and the horizontal component of gravity acting on the plate's mass is negligible compared to the imposed forces at the corners. The 0.0098 N perturbing force was then added to the bottom edge of the plate acting in the $+Z$ direction (the plate is oriented vertically in the XY plane) and was set as a tabular value to remain constant

Table 3 Summary of simulation parameters

Aspect ratio, a/b	Mesh elements	Sub-steps	Applied corner load (N)
1	875	500	20
1.5	1200	250	15
2	1525	250	10
2.5	1850	250	10
3	2150	500	8
3.5	2475	500	7
4	2800	500	6

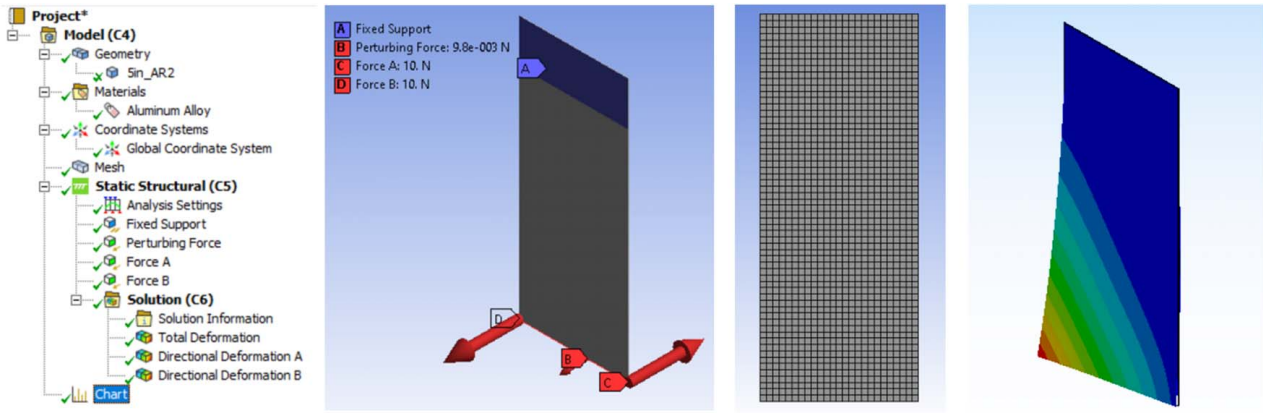

Fig. 5 Static structural simulation study (left), application of boundary conditions and forces (center left), typical mesh (center right), and typical deformation (right)

throughout the simulation. Corner forces were added with the following convention: "Force A" acts on the bottom right "forward corner," pushing the plate in the $-Z$ direction while "Force B" acts on the bottom left "backward corner" by pushing the plate in the $-Z$ direction. These corner forces were of equal magnitude and opposite direction and were ramped over the selected number of sub-steps to the maximum corner load given in the table above. The directional displacement of each corner in the Z axis was measured with a probe and plotted against the ramping force in the chart feature, showing resulting displacement versus the applied load. A plot of total plate deformation with contour lines indicating deflection was inserted to verify the qualitative displacement and buckling of the plate. See Figs. 5 and 6.

3.3 Uncertainty and Limitations. Two interesting features of the curves in Fig. 6 are the minimum displacement for corner A (bottom curve, D) and the knee in the displacement of corner B (top curve, F), which do not actually occur at the same simulated load. The load corresponding to the minimum of corner A was selected as the buckling point for these simulations and it may be the case that reducing the perturbation force to zero will cause the difference in simulated load between these two points to approach zero as well.

4 Results

Note that documentation of raw experimental and simulation data can be provided in .csv format. Figures 7–13 show measured and computed displacements versus load for aspect ratios of 1, 1.5, 2, 2.5, 3, 3.5, and 4.

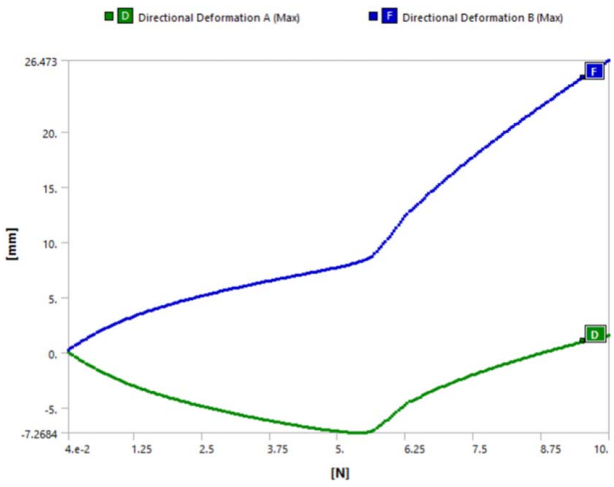

Fig. 6 Static structural simulation study typical chart output

4.1 Dimensional Load Versus Displacement. Clearly, the agreements between experimental and simulation data for aspect ratios 2.5 and 3.5 are not as good for the other aspect ratios (Figs. 10 and 12). There appear to be no physical reasons for this. A modified setup with laser displacement sensors might improve this correlation. However, the general trend is the same in both computations and experiments, with generally weaker quantitative agreement as the aspect ratio increases. This is due to the greater deflection sensitivity of high aspect ratio plates to applied loads and is compounded by difficulties associated with precisely measuring the out-of-plane displacements.

4.2 Nondimensional Buckling Load Versus Aspect Ratio. From Figs. 7–13, the buckling load was estimated and shown in Table 4 and Fig. 14.

The buckling loads shown in Fig. 14 for both the measured and computational results are the best estimates identified by the present authors using the data shown in Figs. 7–13. In Fig. 14, Mg is the applied tip load, b is the plate width, and D is the plate flexural rigidity defined by $D = Eh^3/12(1-\nu^2)$, where E is Young's modulus, h is the plate thickness, and ν is Poisson's ratio. The uncertainty error bars shown in Fig. 14 for the experimental buckling load reflect the uncertainty in the loads applied to the

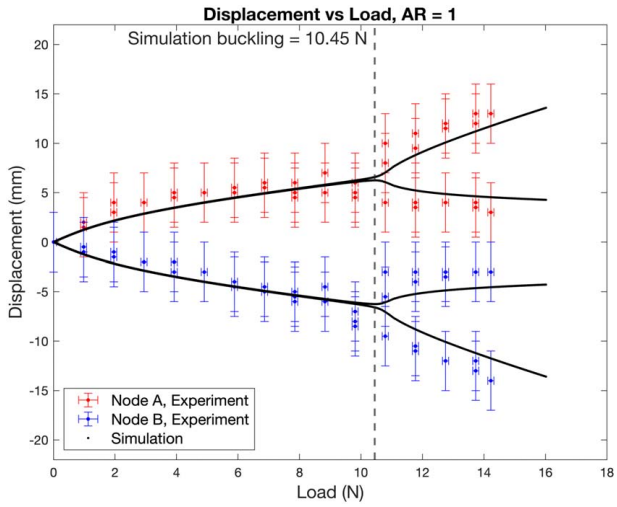

Fig. 7 Experimental versus simulation displacement for the 5 in. (126.21 mm) plate at AR = 1

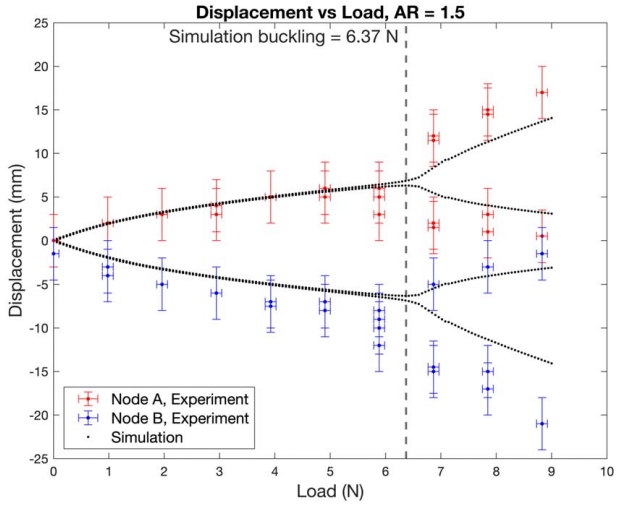

Fig. 8 Experimental versus simulation displacement for the 5 in. (126.21 mm) plate at AR = 1.5

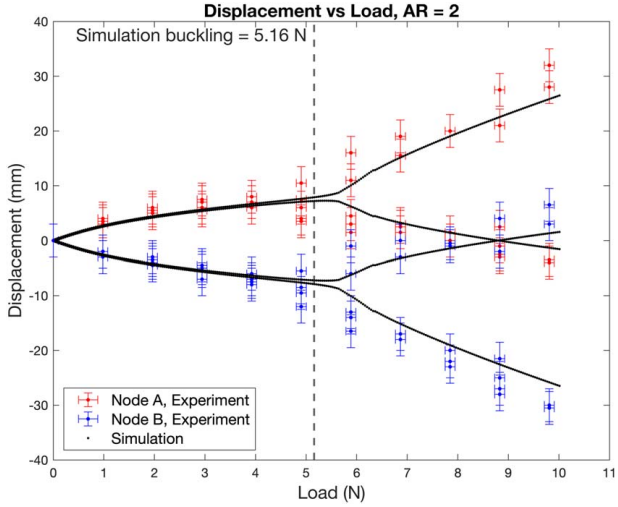

Fig. 9 Experimental versus simulation displacement for the 5 in. (126.21 mm) plate at AR = 2

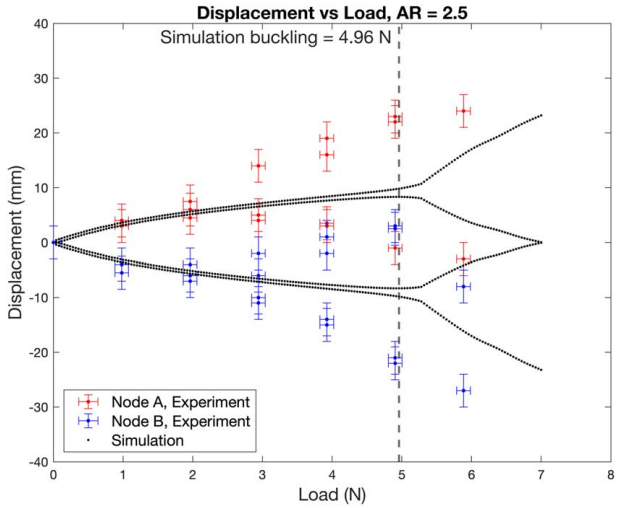

Fig. 10 Experimental versus simulation displacement for the 5 in. (126.21 mm) plate at AR = 2.5

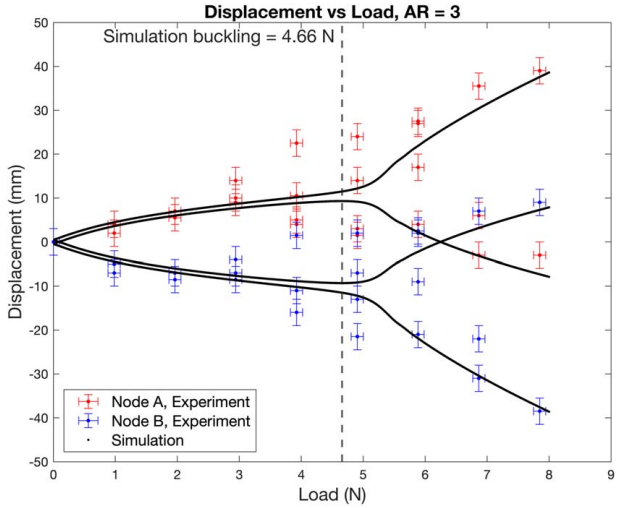

Fig. 11 Experimental versus simulation displacement for the 5 in. (126.21 mm) plate at AR = 3

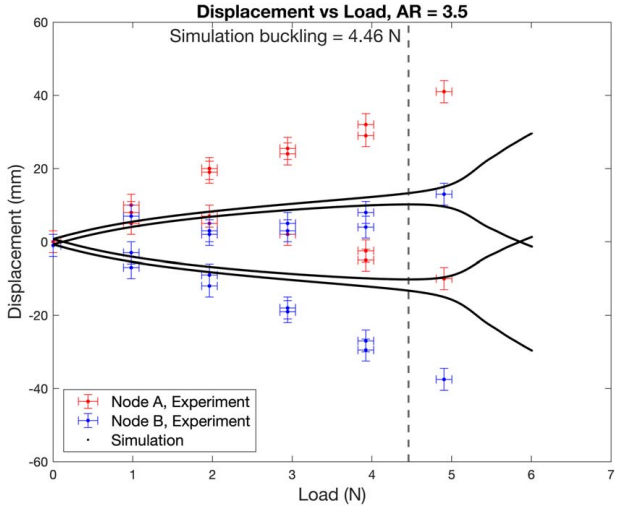

Fig. 12 Experimental versus simulation displacement for the 5 in. (126.21 mm) plate at AR = 3.5

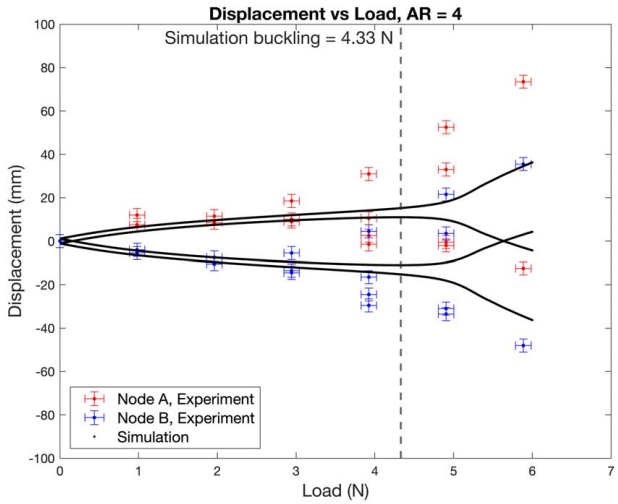

Fig. 13 Experimental versus simulation displacement for the 5 in. (126.21 mm) plate at AR = 4

Table 4 Summary of experimental and simulation buckling loads for the nominal 5 in. (126.21 mm) plate

Aspect ratio	Simulation buckling load (N)	Experimental buckling load (N)
1	10.45	10.30 ± 0.49
1.5	6.37	6.38 ± 0.49
2	5.16	4.41 ± 0.49
2.5	4.96	2.21 ± 0.49
3	4.66	3.43 ± 0.49
3.5	4.46	1.47 ± 0.49
4	4.33	2.94 ± 0.49

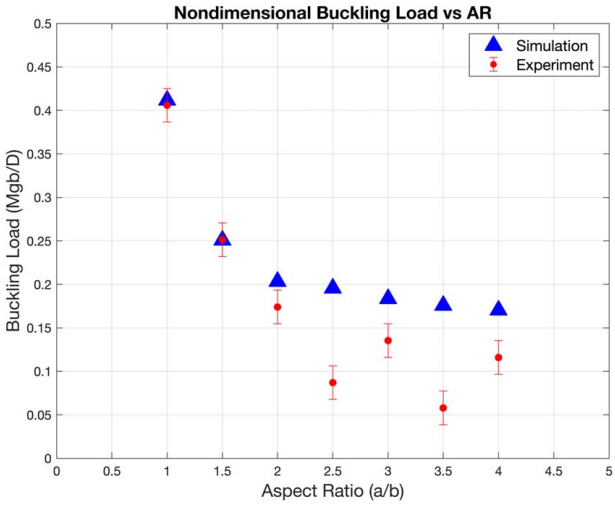

Fig. 14 Experimental and computer simulation buckling loads versus aspect ratio by width for the 5 in. (126.21 mm) plate

experimental plate; specifically, they are equal to the nondimensional load increment of the available mass disks, corresponding to a dimensional 50 g-force. However, as is clear by an examination of Figs. 7–13, there is considerable uncertainty in the judgment required to estimate the experimental onset of buckling. Inevitably there is some subjectivity in identifying the buckling load from both the measured data and the computational data. The reader is encouraged to use their own judgment in the data of Figs. 7–13 to estimate this greater uncertainty in the buckling loads shown in Fig. 14.

5 Conclusions and Possible Future Work

The study of buckling of a vertically mounted cantilevered plate under static torsional loads has led to several interesting results. The prior theoretical prediction of Pai et al. [5] has been confirmed. While there is no analytical predictive model for this buckling phenomenon, the experimental results provide physical insight into the limit cases of the studied configuration. At low aspect ratios, a plate has vanishing length and loses its ability to twist, resulting in higher required nondimensional buckling loads. At these aspect ratios, experimental difficulties include providing sufficiently high corner loads to observe buckling and measuring small corner deflections with high precision. For high aspect ratios, a plate becomes vanishingly narrow, and the twisting moment of applied corner forces decreases. Slight physical imbalances and disturbances in the system result in large out-of-plane nonlinear deflections which become increasingly difficult to measure accurately. This is a noteworthy example where the loading is not obviously an external compressive load yet buckling does indeed occur. A recent paper also considered the appearance of membrane stresses under lateral loading in-plate using an FEA approach [12]. Moreover, the bifurcation that defines the buckling load is about a non-trivial nonlinear equilibrium state.

A quantitative comparison of experimental results with computational results using a theoretical finite element model comparable to that used by Pai et al. has shown a generally good correlation between theory and experiment. Nevertheless, there is an opportunity for improvement in the measurement and loading systems used here. Measuring a complete picture of the deflected plate shapes using digital image correlation would provide further insight into the transition between pre- and post-buckling states. The systems used in the present study were chosen for their simplicity, but more sophisticated measurement and loading devices are certainly worthy of consideration. A corresponding study (the results are not presented here) focusing on the plate mounted horizontally has shown that the effect of gravity is to break the symmetry of the response. In many ways, gravity loads for the cantilevered plate act as the analog of geometric imperfection.

Finally, although this paper focuses on static buckling, it would be interesting to consider dynamics effects. A substantial literature on dynamic buckling can be consulted in this respect. See, for example, Refs. [7,8]. The sudden application of loading (corresponding to a relatively large dynamic perturbation) would result in trajectories undergoing nonlinear transient oscillations before settling onto one of the available equilibrium configurations.

Acknowledgment

The authors would like to thank colleagues for their help in undertaking this work. Diego Salgado Bobadilla and Santiago Brito undertook an experiment on the horizontally mounted plate which provided helpful guidance on how the present experiment was conducted.

Conflict of Interest

There are no conflicts of interest.

Data Availability Statement

The datasets generated and supporting the findings of this article are obtainable from the corresponding author upon reasonable request.

Appendix

Finite Element Convergence Study

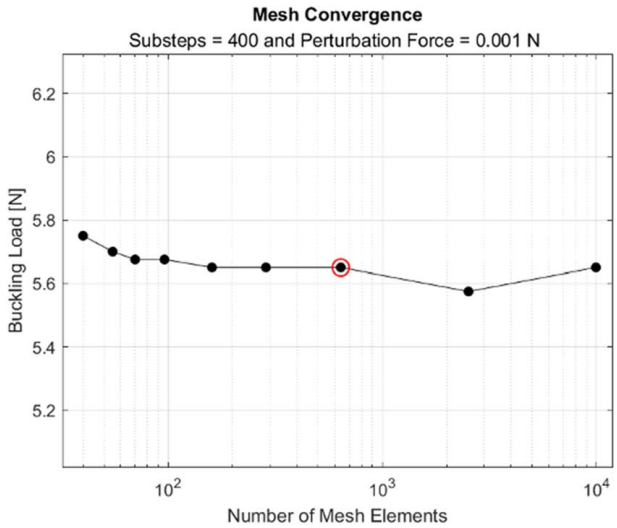

Fig. 15 Mesh convergence, AR = 2 plate. The circled point at 640 mesh elements was selected.

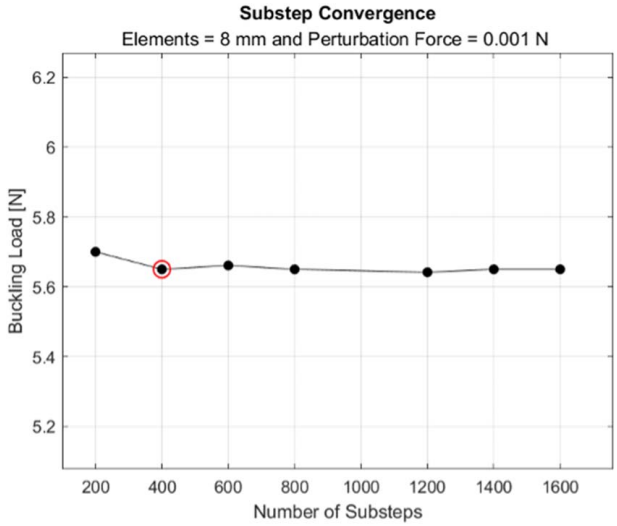

Fig. 16 Sub-step convergence, AR = 2 plate. The circled point at 400 sub-steps was selected.

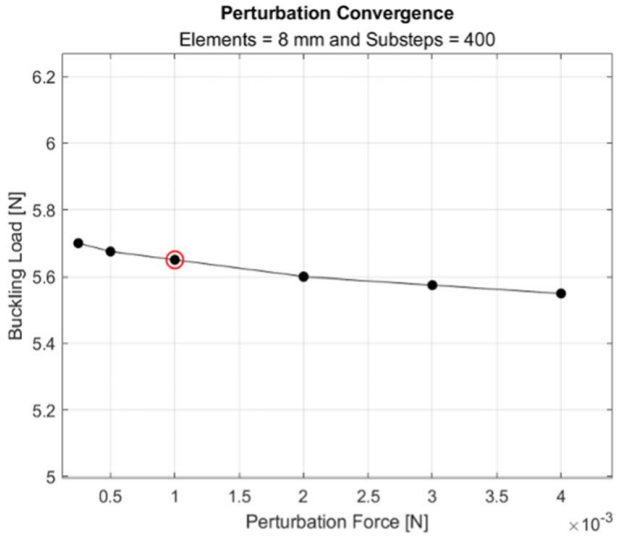

Fig. 17 Perturbation force convergence, AR = 2 plate. The circled point at 0.0098 N was selected.

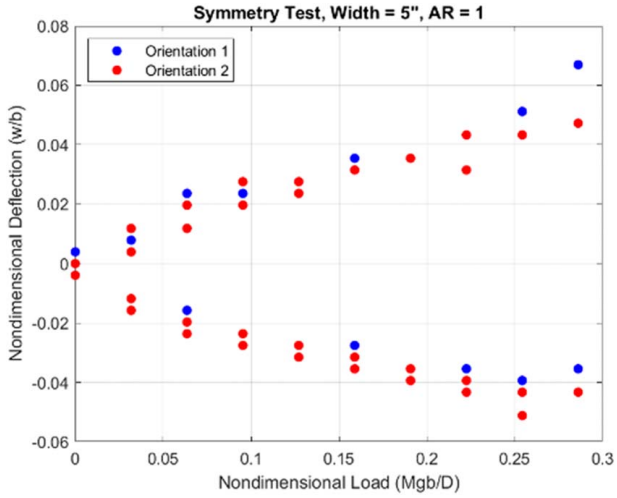

Fig. 18 Symmetry test on experimental rig, AR = 2 plate. The plate is flipped about its vertical axis.

References

[1] Timoshenko, S. P., and Gere, M., 1961, *Theory of Elastic Stability*, McGraw-Hill, New York.

[2] Lachut, M. J., and Sader, J. E., 2013, "Buckling of a Cantilever Plate Uniformly Loaded in Its Plate With Applications to Surface Stress and Thermal Loads," J. Appl. Phys., **113**(2), p. 024501.

[3] Zhang, X., Medina, L., Cai, H., Aksyuk, V., and Espinosa, H. D., 2022, "Kirigami Engineering-Nanoscale Structures Exhibiting a Range of Controllable 3D Configurations," Adv. Mater., **33**(5), p. 2005275.

[4] Reis, P. M., 2015, "A Perspective on the Revival of Structural (in) Stability With Novel Opportunities for Function: From Buckliphobia to Buckliphilia," ASME J. Appl. Mech., **82**(11), p. 111001.

[5] Pai, P. F., Chapman, R. D., and Feng, Z., 2013, "Geometrically Exact Displacement-Based Shell Theory," Thin-Walled Struct., **70**, pp. 1–18.

[6] Virgin, L. N., 2007, *Vibration of Axially-Loaded Structures*, Cambridge University Press, Cambridge, UK.

[7] Bolotin, V. V., 1964, *The Dynamic Stability of Elastic Systems*, Holden-Day Inc., San Francisco, CA.

[8] Chung, M., Lee, H. J., Kang, Y. C., Lim, W. B., Kim, J. H., Cho, J. Y., Byun, W., Kim, S. J., and Park, S. H., 2012, "Experimental Study on Dynamic Buckling Phenomenon for Supercavitating Underwater Vehicle," Int. J. Nav. Archit. Ocean Eng., **4**(3), pp. 183–198.

[9] "Eigenvalue Buckling and Post-Buckling Analysis in ANSYS Mechanical," https://www.padtinc.com/blog/eigenvalue-buckling-and-post-buckling-analysis-in-ansys-mechanical/, Accessed December 9, 2021.

[10] ASM Material Data Sheet, "Aluminum 6061-T6," http://asm.matweb.com/search/SpecificMaterial.asp?bassnum=ma6061t6, Accessed December 9, 2021.

[11] ANSYS WORKBENCH, "Aluminum Alloy Properties. General Materials Library," Accessed December 9, 2021.

[12] Hakim, G., and Abramovich, H., 2022, "Large Deflections of Thin-Walled Plates Under Transverse Loading—Investigation of the Generated In-Plane Stresses," Materials, **15**(4), p. 1577.